Placenta Maps: In Utero Placental Health Assessment of the Human Fetus

Haichao Miao, Gabriel Mistelbauer, Alexey Karimov, Amir Alansary, Alice Davidson, David F. A. Lloyd, Mellisa Damodaram, Lisa Story, Jana Hutter, Joseph V. Hajnal, Mary Rutherford, Bernhard Preim, Bernhard Kainz, and M. Eduard Gröller,

Abstract—The human placenta is essential for the supply of the fetus. To monitor the fetal development, imaging data is acquired using ultrasound (US). Although it is currently the gold-standard in fetal imaging, it might not capture certain abnormalities of the placenta. Magnetic resonance imaging (MRI) is a safe alternative for the in utero examination while acquiring the fetus data in higher detail. Nevertheless, there is currently no established procedure for assessing the condition of the placenta and consequently the fetal health. Due to maternal respiration and inherent movements of the fetus during examination, a quantitative assessment of the placenta requires fetal motion compensation, precise placenta segmentation and a standardized visualization, which are challenging tasks. Utilizing advanced motion compensation and automatic segmentation methods to extract the highly versatile shape of the placenta, we introduce a novel visualization technique that presents the fetal and maternal side of the placenta in a standardized way. Our approach enables physicians to explore the placenta even in utero. This establishes the basis for a comparative assessment of multiple placentas to analyze possible pathologic arrangements and to support the research and understanding of this vital organ. Additionally, we propose a three-dimensional structure-aware surface slicing technique in order to explore relevant regions inside the placenta. Finally, to survey the applicability of our approach, we consulted clinical experts in prenatal diagnostics and imaging. We received mainly positive feedback, especially the applicability of our technique for research purposes was appreciated.

Index Terms—Placenta, Fetal, Flattening, Structure-Aware Slicing, Peeling

✦

1 INTRODUCTION

THE development and functions of the human placenta affect the fetus and, consequently, influence indicators of fetal health such as birth weight and growth [1], prematurity [2], and neuro-development [3]. There is also evidence that assessment of the placenta facilitates predictions of future health problems in adulthood [4]. This vital but barely studied organ controls the transmission of nutrients and hormones from the maternal to the fetal circulatory system and is essential for the fetal immune defense.

Placentas are currently primarily examined **ex vivo** by placing them on a flat table and assessing their structure [5]. The lack of standardized in utero representations of the placenta's structures renders clinical examinations and large population studies a challenging task. Figure 1 shows an ex vivo placenta augmented with a virtual compass for navigation purposes. The ex vivo placenta has predominately a disk-like, flat and round shape [5]. However, due to the limited space in the mother's womb and fetal movements, the placenta is deformed in utero, resulting in a highly diverse shape compared to the ex vivo placenta. As it grows

differently across subjects during gestation, its diversity is increased leading to an unpredictable random shape. This shape heterogeneity is a limiting factor when large population studies are carried out.

In order to enable **in utero** assessment of the human placenta we propose a novel visualization and deliver a proof of concept. On the one hand, conventional slice-by-slice volume inspection is a cumbersome task that requires mental matching of slices. On the other hand, volume rendering provides a good overview, but occlusion requires substantial interaction to inspect the placenta from different viewing angles. A standardized 2D representation would not only facilitate a faster inspection but also a comparison of multiple placentas across subjects. Motivated by standardized visualizations in medicine, such as the *Bull's eye plot* of coronary arteries [6] or CoWRadar of the Circle of Willis [7], we propose a novel standardized representation of the human placenta in utero, referred to as *placenta maps*, mimicking the familiar shape of the placenta ex vivo. The contributions of this paper are the following:

- An automatic identification of the fetal and maternal side of the placenta in utero,
- a structure-aware slicing approach to inspect the interior and exterior of the placenta in a well-defined fashion, and
- a standardized visual representation of the placenta showing the fetal and maternal side in two separate images allowing clinical experts a concise, comparative visual assessment.

In the context of large population studies of the human

- *H. Miao, A. Karimov and M. E. Gröller are with the Institute of Computer Graphics and Algorithms, TU Wien, Vienna, Austria.*
- *M. E. Gröller is also with the VRVis Research Center, Vienna, Austria.*
- *G. Mistelbauer and B. Preim are with the Department of Simulation and Graphics, Otto-von-Guericke University, Magdeburg, Germany.*
- *A. Alansary and B. Kainz are with the Department of Computing at the Imperial College, London, United Kingdom.*
- *A. Davidson, D. F. A. Lloyd, M. Damodaram, L. Story, J. Hutter, J. V. Hajnal, M. Rutherford, B. Kainz are with King's College London, United Kingdom.*
- *E-mail: miao@cg.tuwien.ac.at*
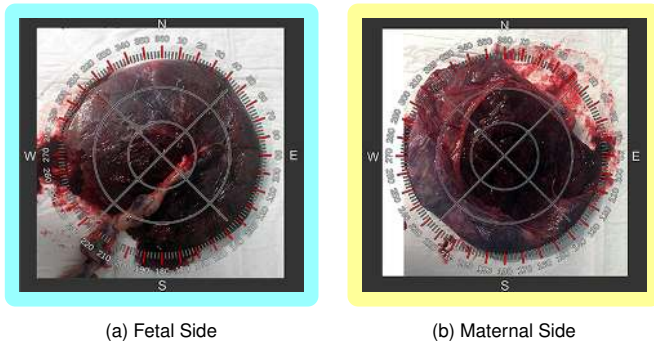
(a) Fetal Side   (b) Maternal Side

Fig. 1. Two photographs of a healthy placenta extracted during a cesarean section. The fetal side is shown in (a) and the maternal side in (b). Since the placenta exhibits a disk-like shape when inspected on a table ex vivo, we decided for a circular visualization using a compass analogy for navigation, as overlaid.

placenta, the proposed approach could serve as a baseline visualization fostering in utero placenta research, as confirmed by our clinical collaborators.

2 RELATED WORK

In order to develop a standardized visualization of a three-dimensional object such as the placenta, a two-dimensional representation of the fetal as well as maternal side is a viable option. The placenta is inspected ex vivo on a table without any further interaction due to the removal of perspective occlusion. To achieve this, a projection from three to two dimensions is required and should be chosen carefully to preserve certain properties of the original object.

The shape of internal organs including the placenta can be highly irregular. Therefore, we need to globally analyze the input shape in terms of geometry. Saroul [8] investigates geometrical properties of two-dimensional surfaces in three-dimensional space. In particular, projection methods between two surfaces are inspected with respect to introduced distortions, e.g., lengths between points in the original surface may change in the projected surface. For medical experts the amount of such distortions is critical, as sizes and positions of anatomical features may not be measured with sufficient precision. Equiareal projections preserve areas of anatomical features across the entire placenta surface and conformal projections preserve orientations of the features with respect to angles. Only developable surfaces can be projected while preserving both areas and angles with isometric projections. Since the placenta surface is not developable in our case, we attempt to reduce both types of distortion, as they influence the interpretation of the data.

In the standard rendering pipeline, several voxels might contribute to a single image pixel of the final two-dimensional representation. To avoid this visual overload, clinical experts rely on two-dimensional slice views of the data. Complex structures of the human body, e.g., heart ventricles, vessel trees, bones in the rib cage region, may be incomprehensible on planar two-dimensional slices. Projection and reformation, as described by Preim and Botha [9], go a step further in terms of complexity and effectiveness. The authors identified three types of projections: anatomical unfolding, anatomical planar reformation or projection, and map projection.

Reformatted images can be computed to alleviate mental efforts and support examination [10], [11]. The reformation process relies on the principle that an arbitrary surface $\mathcal{R}$ can be parametrized with two parameters u, v and then mapped to a rectilinear coordinate system, suitable for common display hardware. The reformation surface $\mathcal{R}$ is often selected in such a way that it passes through relevant anatomical features. Interpretation of the reformation images requires the viewer to understand the location and the shape of $\mathcal{R}$. Therefore, standardization of the reformatted images is important in the medical domain. The technique described by Mistelbauer et al. [11] utilizes a so-called *anatomical layout* in order to connect various branches of a vessel tree. As a result, a medical expert can quickly identify the vessel currently being investigated. Moreover, one can seamlessly browse through the connected vessels.

Kretschmer et al. [10] propose anatomy-driven reformation (ADR), an approach that considers the overall shape of the assessed object for reformation. In this case, the ADR surface coincides with $\mathcal{R}$. They additionally compute offset surfaces in the positive and negative half-spaces of $\mathcal{R}$. These two surfaces represent boundaries of the sub-volume that is being reformatted. With the parametrization of $\mathcal{R}$, this technique tends to preserve the overall shape of the relevant object. The authors use the harmonic triangulation by Floater [12] and iteratively reduce distortions during an as-rigid-as-possible transformation. The step is required as this technique targets objects with different shapes, such as various bones in the human body. The initial harmonic projection reduces distortions in terms of the Dirichlet Energy. This can be thought of as getting a minimally stretched membrane over several protruded objects. While positions of the offset surface are locally optimized in order to minimize distortions, ADR does not explicitly minimize distortions between neighboring reformatted surfaces. This could be disadvantageous when investigating organs where connections between various tissues have to be preserved.

A standardized reformation of the myocardium is presented by Termeer et al. [6]. Representing the volume data with a volumetric *Bull's eye plot*, the technique allows the user to investigate the distribution of scar tissues within the myocardium. The myocardium is unfolded into a cylinder in such a way that all samples from a particular magnetic resonance imaging (MRI) slice, exhibiting a certain distance to the epicardium and endocardium, are arranged into a circle. While the structure of the myocardium may locally vary across different patients, the overall shape of it remains rather constant, leading to a standardized representation for the myocardium.

The visualization techniques described by Kanitsar et al. [13] are designed for reformatting the vascular structures in the human body. While taking the curvature of blood vessels into account, these methods differ in preserved properties. For example, the straightened curved planar reformation (CPR) preserves the length measured along the vascular structures and the stretched CPR leaves the curvatures unchanged. Since these methods require a centerline of the reformatted object they can only be applied to tubular-shaped objects. Vilanova et al. [14] discuss the unfolding of the colon surface. In order to achieve this, the centerline of the colon is extracted. Then, the surface of the

colon is parametrized using 2D coordinates and the unfolded image is generated using nonlinear ray casting. However, this method requires a well-defined centerline.

Krone et al. [15] apply well-known map projections from cartography to the domain of molecular visualization. Using gradient vector flow, they deform an arbitrary molecular surface to a sphere in order to facilitate map projections. Most of the techniques described in this section simplify the display of 3D anatomy in the 2D image space through reformation and projection. Since they cannot directly be applied to the human placenta due to its highly diverse shape, we introduce a flattened view of the placenta surface and allow the user to inspect its interior as well as exterior. Such advanced functionality provides crucial support for placenta research, as stated by our collaborating clinical experts.

3 MEDICAL BACKGROUND

Research on fetal MRI techniques [16] made it possible to image the placenta in greater detail than provided by routine ultrasound (US) examinations at week 12 and 20 of gestation. Besides US, MRI is the second non-invasive option to acquire image data from fetuses in utero, as other possibilities involve ionizing radiation or intervention. T2-weighted MRI has shown to exhibit good tissue contrast for fetal organs in several early studies [16], [17], but additional measurements like diffusion-weighted imaging and the identification of the maternal attachment area are becoming more popular [18].

MRI provides improved contrast and reduced noise in the acquired data of the fetal anatomy to detect abnormalities during pregnancy such as placental pathologies [19]. MRI is also considered to be safe after the first trimester [17] for 1.5 T [20] and 3 T [21] without the use of contrast agents, which may cause teratogenic effects on the fetus. It additionally enables researchers and clinical experts to analyze correlations between the childhood development and different prenatal abnormalities.

Motion corruption limits visual inspection and current visual exploration tools, as depicted in Figure 2. Advanced in utero studies of the placenta in 3D on large populations have not been conducted yet due to this problem [5]. In combination with fast sequences, such an imaging technique plays an essential role in the fetal diagnosis [16], in particular where US fails to provide sufficient data to diagnose certain conditions. MRI acquires high resolution slices from the uterus with a larger field-of-view in comparison to US. Furthermore, the only functional imaging option of US is Doppler imaging. MRI is of special interest because it can image the placenta as a whole, is able to acquire various functional data, and can show structure that is physically impossible to capture with US. However, there are still inter-slice artifacts, which consequently limit reliable diagnostics to individual slices. The observed motion of the placenta is of unpredictable nature, since it consists of maternal respiration movements, fetal movements and bowel movements. Predictable motion, like respiration, can be corrected with image navigator techniques or special MRI sequences [22]. But it is only possible to account for bowel and erratic fetal movements after image acquisition

using heavy oversampling of the input space, slice-to-volume registration, and super-resolution techniques [23], [24].

A quantitative assessment of the placenta is commonly done with respect to its volume. For example, Stevenson et al. [25] present a semi-automatic approach for measuring the volume of the placenta from motion-free 3D US data using a random walker algorithm. This method provides good inter-observer reproducibility, but requires some user interaction and several minutes per segmentation. Wang et al. [26] present an interactive method for placenta segmentation using MRI data, which requires an initial seed-point inside the placenta. Their approach performs well on a small cohort of six subjects, but shows a user-dependent variability in segmentation accuracy. In our work, we use the method presented by Alansary et al. [27] to achieve a motion-compensated segmentation of the placenta. This provides a solid baseline for our proposed standardized visual assessment approach. The achievable reconstruction quality using this approach has been evaluated in detail by Alansary et al. [28].

Image-based diagnostics are usually based on comparing to a memorized or actual *normative* anatomical appearance and on reproducible measurements on these images. Creating a standardized image is difficult for an organ like the placenta and requires specific methods discussed in this paper. The key benefit of *placenta maps* is that it is the first approach that allows the user comparative studies over large populations of placentas. Providing a method that is able to map the placenta into a normative space, primarily facilitates a comprehensive diagnostics of the placenta. Selected example pathologies, where a technique like *placenta maps* will have a direct impact, are twin-to-twin transfusion syndrome (TTTS), preeclampsia, preterm birth, and stillbirth. The visualization of relevant biomarkers, such as the overall appearance, texture, lesions, functional properties, and measurement of the attachment area, is eased through our approach. In clinical literature [29], [30], such biomarkers are considered to be vital measurements to assess the likelihood of complications during pregnancy.

Our collaborating clinical experts apply MRI to investigate TTTS. This syndrome is specific to monochorionic twins gestations, since the blood supply could be imbalanced and one of the twins is insufficiently supplied from the single shared placenta. In the case of TTTS the vessels branching off the two umbilical cords are interconnected with each other. TTTS is treated with endoscopic laser surgery to interrupt the vessel communications. Without intervention this syndrome is lethal to either one or both twins.

Cotyledons are small lobules that cover the entire maternal side, as shown in Figure 1b ex vivo. Ten to 40 cotyledons [5] are attached to the uterine wall and are responsible for the exchange of oxygen and nutrients between fetal and maternal blood. Because of the crucial function of cotyledons, they are of particular interest when examining the in utero placenta.

4 METHODOLOGY

In order to mimic the ex vivo assessment of the placenta we propose a novel visualization approach, outlined in Figure 3. It consists of the following four major automatic

(a) Motion-corrupted cutting planes
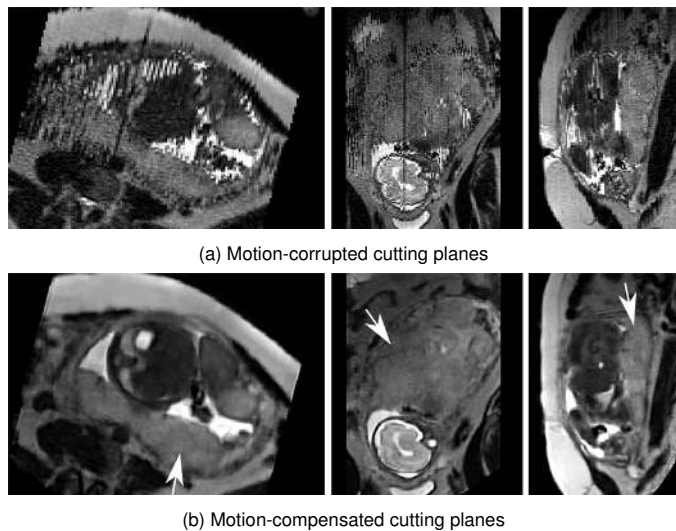

(b) Motion-compensated cutting planes

Fig. 2. Three orthogonal cutting planes through a motion-corrupted dataset of T2-weighted MRI slices covering the uterus at a gestational age of 33 weeks are presented in (a). The motion-compensated reconstruction of the dataset [23] is shown in (b). The placenta is depicted by the white arrows.

steps: segmentation, slicing, splitting, and visual mapping. Firstly, the placenta is segmented and secondly, a distance field and its iso-surfaces are created. In the third step, the fetal and maternal side are automatically identified and fourthly, both three-dimensional meshes are projected into two-dimensional space. This workflow offers a standardized layout, and also favors inter-subject comparison. Subsequently, each step is explained in detail.

4.1 Segmentation

The input datasets were acquired by a 1.5 T Philips Achieva MRI system using a 32 channel cardiac array for signal reception. A total of four placentas with gestational age ranging from 24 to 37 weeks were motion-compensated by the technique of Kainz et al. [23] and segmented using the approach of Alansary et al. [27]. The resulting motion-compensated placenta masks are defined on a $0.75 \times 0.75 \times 0.75$ mm volumetric lattice and are shown in Figure 3 in the segmentation step.

We post-process the segmentation masks by applying a morphological opening with a spherical structuring element of radius five voxels to remove small local noise and objects. Afterwards, we perform morphological closing to fill small holes, again with a spherical structuring element but of radius ten voxels. The final mask of the placenta is then used in the subsequent steps.

4.2 Structure-Aware Slicing

Motivated by traditional axial, sagittal, and coronal slicing through the data for exploratory purposes, we apply this concept to the structure of the placenta itself. Instead of slicing along a defined axis, we compute the Euclidean distance field from the surface $\mathcal{R}$ of the placenta using the method described by Danielsson [31].

We then compute offset surfaces of $\mathcal{R}$ at discrete distances of 1 mm. Since these surfaces define layers, we denote $\mathcal{R}$ with $\mathcal{L}_0$, the surfaces inside the placenta with positive indices
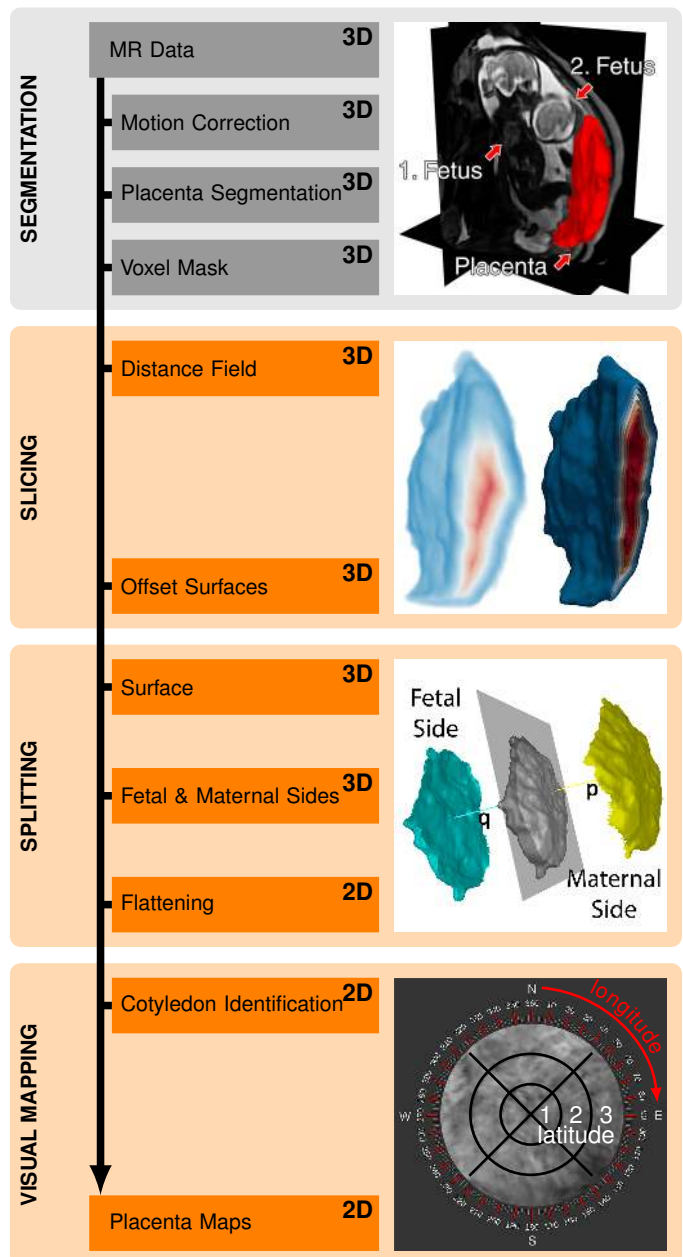

Fig. 3. Our automatic pipeline consists of four steps. *Segmentation* generates the mask for the placenta. *Slicing* creates the layers based on the placenta structure. For demonstration purposes we slice every 2 mm. *Splitting* separates the layers into a fetal and maternal side and each is then flattened. Finally, *Visual Mapping* creates a standardized view of the isolated placenta. Each location on the fetal and maternal side can be addressed with latitude $(1-3)$ and longitude $(1° - 360°)$ coordinates using the compass overlay.

and the ones outside with negative indices. The layers are illustrated in Figure 4. Slicing into the placenta is practical, as it reveals the interior layer by layer. However, we also provide means to display the context of the placenta by slicing outside of the placenta. With outside slicing, we can visualize the uterine wall on the maternal side and the amniotic cavity on the fetal side with respect to the placenta structure. The slicing leads to a set of layers $\mathcal{L}_i$, each consisting of a set V of vertices $v_k \in \mathbb{R}^3$ and faces $f_j \in F$. The image of the slicing step in Figure 3 shows the distance field on the left as well as the internal layers on the right.
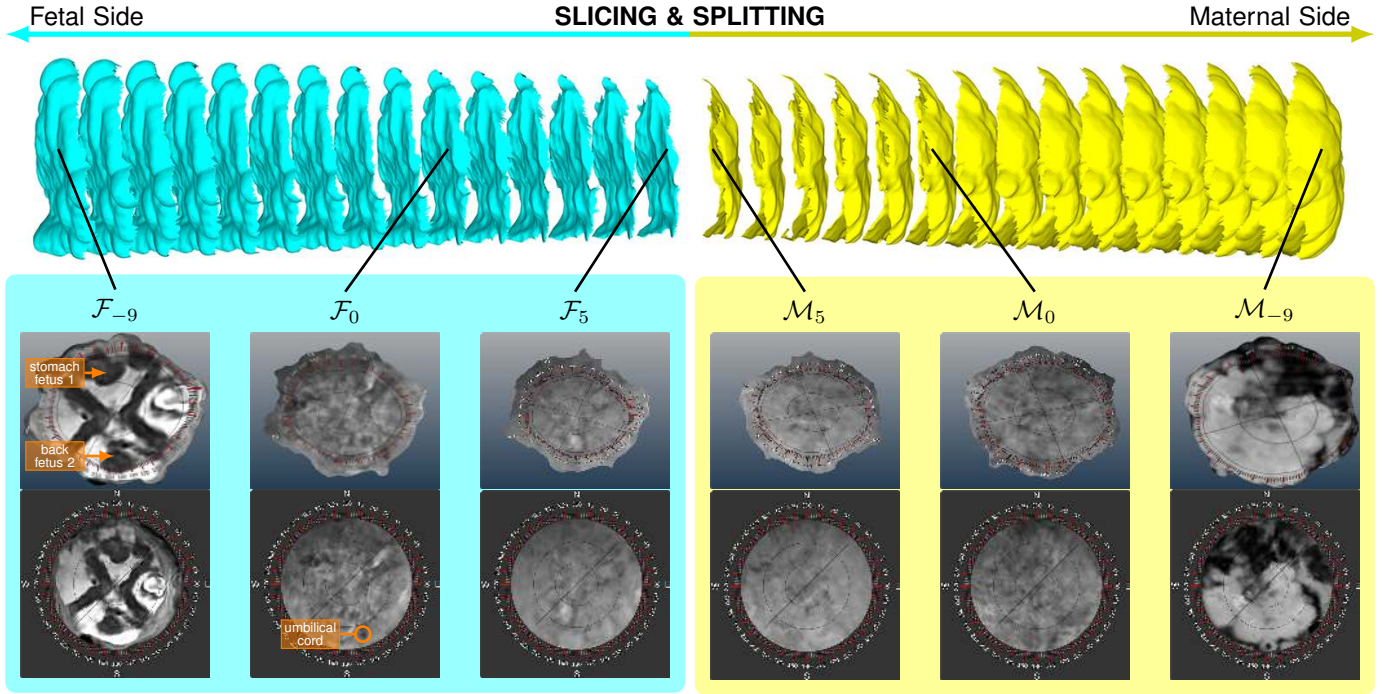
Fig. 4. The layers of the placenta. First, the layers $\mathcal{L}_{-9} \ldots \mathcal{L}_5$ are split into a blue fetal side ($\mathcal{F}_{-9} \ldots \mathcal{F}_5$) and a yellow maternal side ($\mathcal{M}_{-9} \ldots \mathcal{M}_5$). Layers are shown in 3D and at the bottom in the standardized, flattened view. In 3D, it can be seen that the shape gets smaller and smaller as layers are removed. $\mathcal{F}_{-9}$ shows the two twins. The structural appearance in $\mathcal{M}_0$ (maternal) indicates the cotyledons.

In contrast to our approach, the ADR technique by Kretschmer et al. [10] uses the normal vectors of a surface to compute its offset surfaces. However, this possibly leads to self-intersections and not well-defined surfaces, especially in regions with high curvature or in case of large offsets. Using a distance field, we avoid these types of problems.

Since we flatten each layer in the subsequent step and provide a two-dimensional map, the user can scroll through the different layers of the placenta in the usual fashion. This offers the possibility to see structures at a certain depth or height, such as vessels, cotyledons or diseased tissues.

4.3 Splitting

We divide each extracted layer into two parts that reflect the fetal and maternal side as shown in the splitting step in Figure 3. We refer to this fetal and maternal side detection as simply splitting.

As we rely on a coarse orientation of the placental shape, we perform principal component analysis (PCA). The basic idea is to consider the vertices of the layer $\mathcal{L}_i$ as a set of 3D points that is projected into a linear subspace. This resembles fitting a plane to the surface, where the two axes of the plane describe the direction of the highest and the second highest variance in terms of mesh point positions. The best fitting plane is found by using a linear least-square fitting method, which minimizes the sum of squared distances from all points to the plane, as shown in the image of the splitting step in Figure 3. As the normal vector $\mathbf{p}$ of this plane represents the direction of the least variance, it reflects the thickness of the placenta. Vector $\mathbf{q}$ is defined as the opposite of $\mathbf{p}$.

In order to split $\mathcal{L}_i$ into two parts $\mathcal{F}_i$ and $\mathcal{M}_i$, we first find two faces f_A and f_B such that $f_A \in \mathcal{F}_i$ and $f_B \in \mathcal{M}_i$. They are found by intersecting the mesh with a line defined

by the vectors $\mathbf{p}$ and $\mathbf{q}$ and a point O at the or close to the center of the placenta. We set the origin of our coordinate system to this point. Consequently, O has to be located inside the placenta at a central position. We define O as a single member of the skeleton S that minimizes the sum of distances to the remaining skeleton points. We apply the voxel-based skeletonization approach by Lee et al. [32] that uses topological thinning to extract the skeleton S of an object. From the skeleton voxels we find O as follows:

$$O = \arg \min_{X \in S} \sum_{R \in S} \|X - R\|_2. \tag{1}$$

This formula is based on the geometric median, however, it minimizes the sum of distances to a member of the skeleton. As O is located on the skeleton of the placenta it is ensured that O is always located inside the placenta. This is not guaranteed if the centroid or the center of mass is used. They could lie outside the shape if the in utero placenta is concave, which is rather common.

To separate $\mathcal{L}_i$ into the two parts $\mathcal{F}_i$ and $\mathcal{M}_i$ corresponding to the fetal and maternal side, we combine the *silhouetteness* property of faces with their breadth-first traversal. We construct a graph where vertices are mesh faces and edges connect adjacent faces. The faces f_A and f_B are the starting points of the breadth-first traversal. During the traversal, all neighboring faces of f_j are visited first and with each face, the cost of 1 is added to include the approximate distance to f_A and f_B. This way we guarantee that each part is a connected set of faces, which is a requirement for the flattening. For each face f_j we compute two costs, i.e., one for belonging to the fetal part $c_{\mathcal{F}}(f_j)$ and one for belonging

to the maternal part $c_{\mathcal{M}}(f_j)$:

$$f_j \in \begin{cases} \mathcal{F}, & \text{if } c_{\mathcal{F}}(f_j) < c_{\mathcal{M}}(f_j) \\ \mathcal{M}, & \text{otherwise} \end{cases}, \qquad (2)$$

$$c_{\mathcal{F}}(f_j) = c_{\mathcal{F}}(f_{j-1}) + s(\mathbf{n}(f_j), \mathbf{q}) + 1, \qquad (3)$$

$$c_{\mathcal{M}}(f_j) = c_{\mathcal{M}}(f_{j-1}) + s(\mathbf{n}(f_j), \mathbf{p}) + 1, \qquad (4)$$

$$c_{\mathcal{F}}(f_0 = f_A) = 0, \quad c_{\mathcal{M}}(f_0 = f_B) = 0, \qquad (5)$$

$$s(\mathbf{n}(f_j), \mathbf{v}) = \angle(\mathbf{n}(f_j), \mathbf{v}). \qquad (6)$$

where $\mathbf{n}(f_j)$ denotes the normal to the face f_j and $c_{\mathcal{F}}(f_{j-1})$ and $c_{\mathcal{M}}(f_{j-1})$ are the costs of the previously traversed face f_{j-1}. The underlying idea of the silhouetteness term $s(\cdot)$ is that f_j is more likely to belong to $\mathcal{F}$ if $\mathbf{n}(f_j)$ is aligned with $\mathbf{q}$. Therefore, we use the angle between $\mathbf{n}(f_j)$ and $\mathbf{q}$, which is motivated by the common approach to detect silhouettes in rendering. The silhouetteness term $s(\cdot)$ measures the angle in radians. The cost is increased by 1 if $\mathbf{n}(f_j)$ points in the same direction as $\mathbf{q}$ and by $1 + \pi$ if the two vectors have opposite directions. If only the *silhouetteness* term is considered, local curvature changes may cause the assignment of the faces to the wrong side due to the change of face normals. By accumulating the costs, we ensure that f_j is connected to f_0 inside either $\mathcal{F}_i$ or $\mathcal{M}_i$. This means that the more distant f_j is to f_0, the higher is the cost. These two terms ensure that crossing from one side to another is very costly. This splitting of the initial surface into two parts is shown in the splitting step of Figure 3 and in Figure 4.

We compute which of the sides is the fetal and which is the maternal one. Anatomically, the fetal side is proximal, i.e., facing towards the body center, and the maternal side is distal, i.e., facing away from the body center. The proximity is estimated with respect to the volume center. We can safely assume that the fetus is located in the volume center, as it coincides with the region of interest during the data acquisition of the fetal MRI.

In the case that the principal component analysis (PCA) fails, e.g. if the input shape is sphere-like, which is unlikely, then we suggest a fallback solution: the user can manually specify f_A and f_B. The remaining splitting step would still be automatic.

Flattening

The surface of the placenta can exhibit large local curvature. This hampers its investigation in conventional slice views commonly used by the clinical experts. Following the standard procedure of physical examination of the placenta ex vivo, we ease the exploration of the placenta in utero by flattening it. As a result, we create a standardized view of the placenta, as shown at the bottom of Figure 4.

Our method is based on the fact that the ex vivo placenta can be physically deformed into a disk shape (see Figure 1). The clinical experts distinguish between the fetal and the maternal side of the placenta. Therefore, we split the original placenta surface into these two parts and flatten each part separately. Because of the disk shape, we do not need additional transformations after we flatten the surface with the *mean value coordinates* approach of Floater [33]. In this flattening, the original in utero shape information is lost. However, the specific placenta shape is functionally not important [5]. The surface $\mathcal{P}$ must be open, which we achieve by splitting the entire layer into two parts as described in subsection 4.3. The boundary points of the surface $\mathcal{P}$ are mapped to a disc. Projections of the remaining points are then determined inside the disk via the convex combination mapping. The convex combination mapping utilizes the mean value coordinates of each point in the convex basis formed by neighboring points [33]. After the flattening we refer to the flattened fetal and maternal side as $\mathcal{F}_i'$ and $\mathcal{M}_i'$ respectively. The faces that form the corresponding meshes are denoted as f_j'.

In Figure 5 we map a checkerboard pattern onto the placenta surface to show the angular distortion between the original and the flattened meshes. To quantify the area distortions, we compute the relative face-area deviation and color-code it. The area deviation of a face f_j is thereby computed as follows:

$$\eta(f_j') = \frac{|A(f_j') - A(f_j)|}{A(f_j)}, \qquad (7)$$

where $A(f_j)$ denotes the area of f_j.

4.4 Visual Mapping

A placenta map is a visualization that consists of two views, as shown in Figure 4. The first view is a 3D visualization of placenta layers and the second one is the separate flattened reformatted visualization of the fetal and maternal sides. In the last image of Figure 3, we overlay a compass onto the maternal side for navigation purposes. The compass divides each side into four quadrants. Each quadrant is specified by a cardinal direction (north, east, south and west) for a rough guidance. For a more accurate addressing, latitude $(1 - 3)$ and longitude (between $1°$ and $360°$) coordinates are used. For example, in the first two images of Figure 5 the red part is marked at $(2, 315° - 45°)$. This specifies a latitude of 2 with a longitude between $315°$ and $45°$. The compass is thereby standardized and overlaid over the 3D and 2D view. This enables experts to mark diseased portions on the placenta utilizing a link between the 3D and 2D view.

This way we present the fetal and maternal side simultaneously without occlusion as shown in Figure 5. By traversing all layers, the clinical expert can quickly browse through the placenta and investigate its interior with an easier navigation in reformatted and standardized images than in conventional slice views.

Using standardized flattened views, the comparison of multiple placentas becomes feasible. The overlaid compass can be reoriented manually to match several placentas. The comparison of placentas from different patients or multiple time-stamps of the same patient is an interesting extension to existing methods in placenta research. It may reveal new insights about diseased regions and their influence during the gestation. In order to enable the comparison, we juxtapose the flattened placenta images. Using the compass overlay, the expert can match regions on the flattened images from different subjects and time-stamps. With slice views or volume rendered images, such a comparison is rather difficult, because the placentas vary significantly in shape. Thus, the mapping between two or more placentas is too complicated to easily support a mental model.

Clinical experts can potentially investigate diseases, such as TTTS, and track vessels on the fetal side. Having just
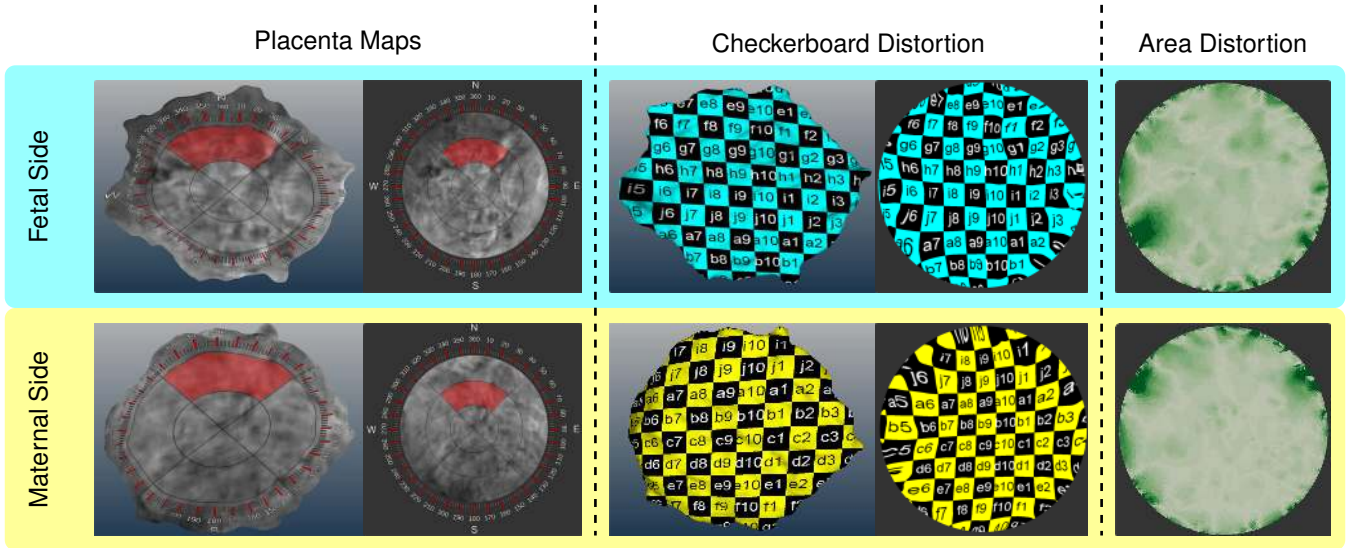
Fig. 5. Flattening of the fetal and maternal side. The images on the left show the placenta maps of the fetal as well as maternal side. A compass is projected onto both sides in 3D and 2D. Two areas highlighted in red correspond to each other. In the central images, a checkerboard pattern is orthogonally projected along $\mathbf{p}$ to demonstrate the angular distortion between the 3D and 2D views. $\mathbf{p}$ is then aligned with the direction to the viewer. On the right side, the area distortion $\eta(\cdot)$ is shown per face, with colors ▢▨▨▨▨ representing the intervals $[0; 0.2), [0.2, 0.4), [0.4, 0.6), [0.6, 0.8), [0.8, +\infty)$ respectively.

conventional slice views, the expert would need to build up a mental model of the placenta and its vascular structures. Our technique shows in 2D and at once the entire fetal side where the vascular structures are located. The vessels inside the placenta could be easily investigated with our structure-aware slicing method.

5 IMPLEMENTATION

Placenta maps use the Qt, the ITK, and the VTK framework, executed on an Intel Core i7 CPU with an NVidia GeForce 980 Ti GPU. The structure-aware slicing and splitting are performed on the CPU. For the mean value coordinates technique and the PCA we use the CGAL library [34]. In order to provide an interactive investigation of the data, the layers of the placenta are automatically flattened beforehand.

6 RESULTS AND DISCUSSION

In this section, we demonstrate our approach on three datasets, shown in Figure 4, Figure 6 and Figure 7. Each dataset is discussed and we explain how potential findings can be achieved using placenta maps. We also discuss how to simulate cotyledons and how our slicing displays them.

The placenta of a subject at a gestational age of 26 weeks having monochorionic twins and the diagnosis of TTTS is shown in Figure 4. The top image depicts the segmented placenta and an exploded view of our structure-aware slicing method with the split fetal and maternal side. Layer $\mathcal{F}_{-9}$ displays both twins, the first twin is located at the north in the placenta map and the second twin is partially visible at the south. As the twins are visible on the fetal side, this suggests that our automatic splitting technique correctly classifies both, the fetal and maternal side. $\mathcal{F}_0$ and $\mathcal{M}_0$ show the initial surface of the segmented placenta. Within our proposed placenta map in $\mathcal{F}_0$ the suspected umbilical cord insertion is visible at $(3, 160°)$. In the maternal layer $\mathcal{M}_0$,

the cotyledons are depicted, though in low detail due to yet insufficient quality of the data acquisition. $\mathcal{F}_5$ and $\mathcal{M}_5$ display internal tissues of the placenta. The placenta maps allow physicians to monitor the development of the in utero placenta in a standardized way.

Another subject at a gestational age of 30 weeks is presented in Figure 6. Earlier occurrence of the TTTS is suspected in this subject, but laser surgery was not applied. One twin died in week 23, but the other survived. The uterine wall is partially depicted in $\mathcal{M}_{-10}$. The surviving twin is visible on the entire placenta map in $\mathcal{F}_{-10}$. Amniotic fluid appears as bright matter, exhibiting high intensity values and surrounding the twins. In $\mathcal{F}_{-10}$, showing the amniotic cavity, the umbilical cord of the surviving twin can be seen in the East quadrant, precisely at $(2, 45° - 160°)$. The insertion of the cord on the fetal side at $\mathcal{F}_0$ is at $(2, 45°)$.

The last subject is at a gestational age of 37 weeks and shown in Figure 7. Although the placenta is healthy, the subject suffered a cytomegalovirus infection, causing microcephaly in the fetus. The anatomical context at $\mathcal{F}_{-10}$ displays the fetus. This indicates the correct automatic splitting of the placenta into the fetal and maternal side. At $\mathcal{F}_0$ the insertion of the umbilical cord to the fetal side is at $(2, 140° - 150°)$. Cotyledons appear on the maternal side $\mathcal{M}_0$. $\mathcal{F}_3$ and $\mathcal{M}_3$ present slices inside the placenta. Here, vessels branching from the umbilical cord can be observed at $(2, 160°)$ in $\mathcal{F}_3$.

Figure 8 depicts **artificial cotyledons**. Since the fetus is focused during the data acquisition, the signal-to-noise ratio of the placenta is low. This makes the visual assessment of the placenta a challenging task, especially of structures with low contrast, such as the cotyledons. Our collaborators explicitly want cotyledons in the visualizations to gain an understanding of the uterine attachment when using placenta maps. In order to demonstrate such functionality, we artificially created cotyledons in a concept study. Based

on the ex vivo appearance of cotyledons, we modeled them as spheres with center points on the maternal side. The intensity values of the voxels inside a cotyledon are defined as $I = [1 - (d/r)^s] \cdot 2000$, where d is the Euclidean distance to the center of the sphere and s controls the fall-off in intensity values. We empirically set radius r to 25 voxels and s to 1.7. The pattern of the cotyledons remains stable with respect to the layer depth. Hence, our technique shows internal structures with rather small distortions between adjacent layers.

7 EVALUATION

To assess the applicability and acceptance of the proposed technique to in utero examination of the placenta, we conducted a survey. It was based on questions with answers on a five-point Likert-scale and open questions. The questions were grouped into the following three core aspects of our technique: structure-aware slicing, comparability, and flattening. The first part of the survey consists of pre-recorded (R) videos that demonstrate the technique to the clinical experts. The videos showed the three aspects separately and the experts rated their usefulness. To assess the acceptance of our technique, we designed the second part of the survey to be interactive (I). The experts tested our tool with multiple datasets and rated the usability of the same three aspects. Finally, the participants assessed the overall readability of placenta maps. We asked summary questions regarding the applicability of our technique to placenta research and also to clinical routine. Figure 9 depicts the results of the survey, where the answers from the pre-recorded (R) and the interactive (I) presentation of the aspects are separated. For the pre-recorded part, we received four responses from clinical experts, where three are radiologists specialized in prenatal diagnostics and one is a pediatrician. The interactive part of the survey was conducted by three experts.

Our proposed **structure-aware slicing** was rated by the experts with a score of 4.4 (R) and 4.0 (I). The experts especially appreciate the ability to display the isolated placenta and the slicing in order to see the internal tissues layer by layer with little mental effort. We assume, this offers the experts an efficient way to go through the different tissue layers. One expert stated that our slicing approach is very promising for tracking blood vessel, e.g., in case of TTTS.

The **comparability** of our standardized visualization got the best scores among the three aspects, with 4.3 (R) and 5.0 (I). The increase of the score after the experts tested the tool shows that this is the most valued aspect of placenta maps. Also, the qualitative feedback so far was clearly indicating that this feature is very important if a large number of placentas has to be investigated within a study. Ultimately, we aim to provide quantitative measurements and comparisons of the fetal and maternal sides.

We get a 2D view of the fetal and maternal side with **flattening** at the expense of accuracy, since each side is distorted as shown in Figure 5. This feature was rated with scores of 4.2 (R) and 4.3 (I). From the earlier qualitative feedback of one of the experts, we know that this feature can be very useful for placenta research, as it provides a fast overview of the fetal and maternal side. We quantify the introduced distortions later in Figure 10 to validate our
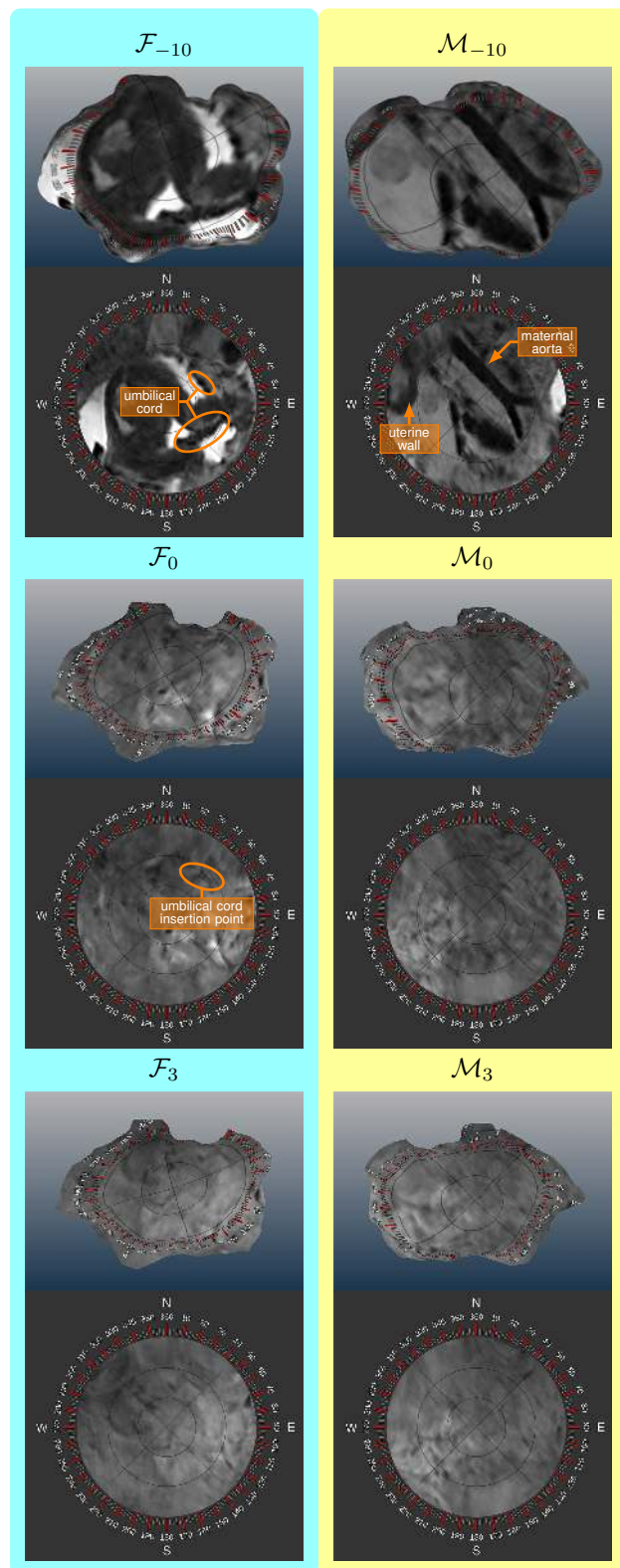

Fig. 6. Subject at a gestational age of 30 weeks with twins. The placenta map $\mathcal{F}_{-10}$ shows the context of the placenta where the surviving twin is visible. The amniotic fluid has high intensity values, mapped to white. The layer $\mathcal{F}_0$ displays the surface of the fetal side, where one umbilical cord is visible as a dark spot. $\mathcal{F}_3$ and $\mathcal{M}_3$ show the internal tissues of the placenta when three layers are already removed. The three-dimensional views clearly show the decrease of the layers in size caused by their successive removal.
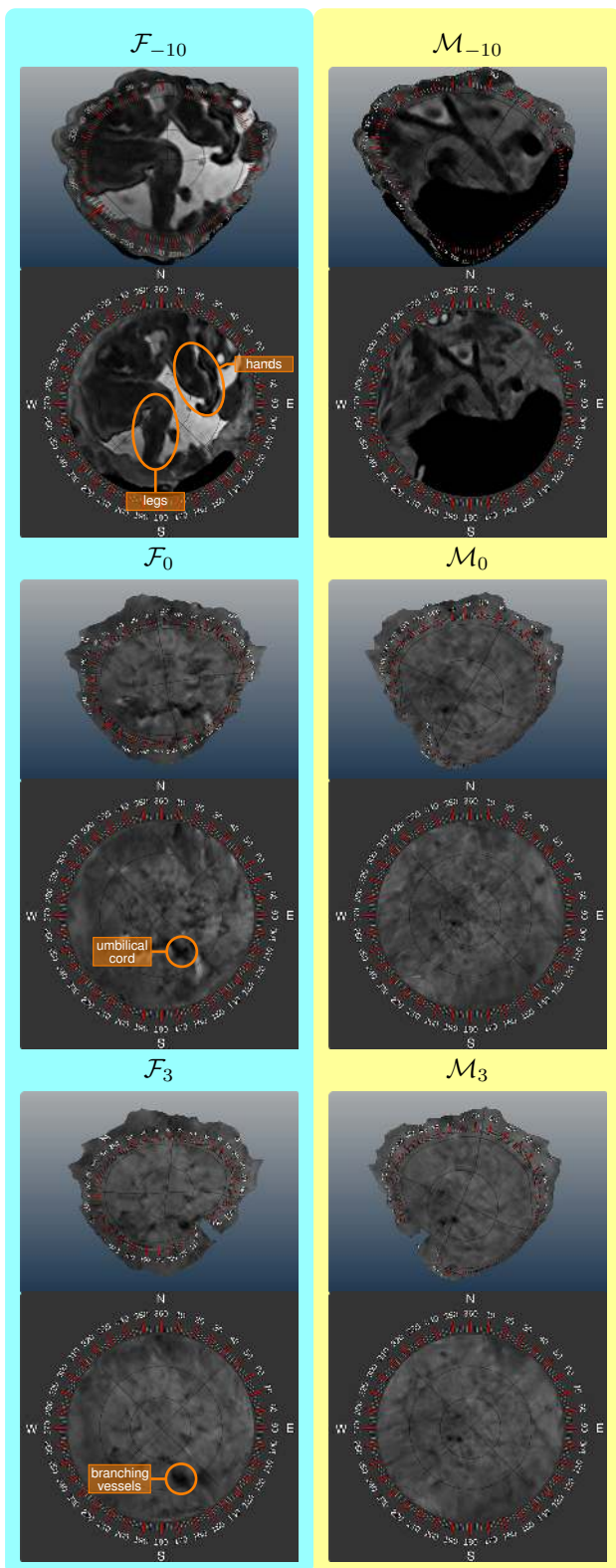
Fig. 7. Subject at a gestational age of 37 weeks with a healthy placenta, but suffering from an infection. $\mathcal{F}_{-10}$ and $\mathcal{M}_{-10}$ display the context of the placenta and clearly delineate the fetus in the amniotic cavity in $\mathcal{F}_{-10}$. This indicates that our splitting approach correctly detected the fetal and maternal side. $\mathcal{M}_0$ shows the surface of the placenta with cotyledons in low detail on the maternal side. $\mathcal{F}_3$ and $\mathcal{M}_3$ display the internal placenta tissues, after removing three layers.
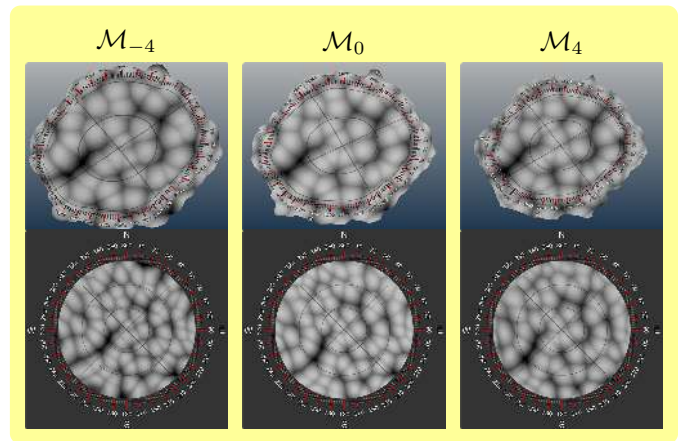

Fig. 8. Artificial cotyledons modeled as spheres across the maternal side of the placenta. The different layers demonstrate the depth of the artificial cotyledons.

flattening technique. To satisfy the clinical requirements concerning accuracy, we additionally display axial slices that are linked to the placenta maps and the 3D view, as shown in the segmentation step of Figure 3.

The **overall readability** of our method received a score of 4.3, but could be improved. We suspect that the readability is attributed to our compass overlay, which is a novel way to address the heterogeneous placenta surface and, as stated by one of the experts, needs some familiarization time.

Regarding the **clinical applicability**, our technique got a score of 4.5. While the radiologists in general gave better ratings, the lowest rating of three was given by the pediatrician. We assume that this is attributable to the fact that he is less experienced with reading MRI data than radiologists.

The **research applicability** was rated with the best scores of five from all participants. According to one of our experts, the attachment to the uterine wall is of potential interest. However, a large number of placentas will have to be investigated, which would be feasible with placenta maps. The high rating gives a clear indication that our technique has potential to be applied in the research of placentas, which has been the main motivation of our approach.

In the open questions part of the survey, we asked the participants about their preferences, shortcomings of the technique, and further suggestions. We inquired which **different diseases and conditions** could be investigated with placenta maps. TTTS, placental infarction, previous laser treatment, and placenta praevia has been mentioned by two participants.

Regarding the **preferences**, two experts liked the possibility to compare multiple placentas enabled by our standardized, flattened views. Two participants appreciated the compass overlay on the placenta and consider this feature useful to visualize diseased portions.

Regarding the **shortcomings**, all experts agreed that the signal-to-noise ratio of the original data is insufficient for perceiving the features of interest, such as cotyledons and vessels. The primary cause of this issue is the used MRI sequence that does not target the placenta tissues specifically.

We also got **suggestions for improvement**. One expert recommends to enhance the segmentation result before mapping it to a 2D structure. This concerns the quality of
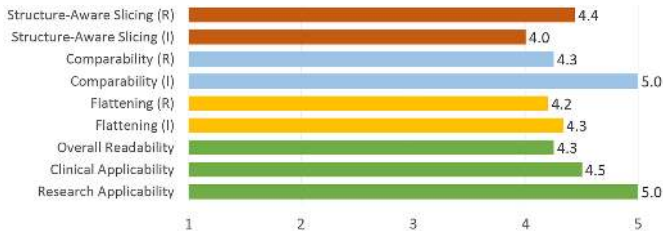
Fig. 9. The outcome of the survey. We differentiate between a pre-recorded (R) and an interactive (I) part. The scores are from one being poor to five being excellent.

Fig. 10. Distribution of area deviation $\eta(\cdot)$ of all presented datasets. Most faces exhibit a low distortion in the interval of $[0, 0.2)$.

the data, but not our technique. The clinical experts were convinced that with an improved signal-to-noise ratio of the data our technique would be highly relevant for research purposes and also for clinical use cases. The participants consider it useful to segment the umbilical cord and the cotyledons. The measurements of linear sizes were also an interesting suggestion, since they could improve the compass overlay to be applicable for quantitative measurements.

The flattening inevitably introduces some distortions. After interacting with our tool, we interviewed three experts regarding the acceptance of these distortions for clinical and exploratory usage. In the **clinical use case** the distortions are regarded as very acceptable, especially if the inspection only concerns the quantification of areas and counting cotyledons. The participants stated that our technique is much more useful than cutting planes. However, the simultaneous display of the undistorted view is necessary to provide the relationship to the unchanged anatomy. In the **exploratory use case**, the distortions are definitely acceptable for the intended purposes. One expert stated, that this technique is exactly what clinical research of the placenta currently needs. An appropriate training is deemed necessary in order to fully understand the placenta maps. In conclusion, it seems that the benefits of standardization, comparability, and fast assessment of unusual placentas outweighs the distortions introduced by our approach.

We quantified the distortions in all presented datasets using the distribution of **area deviations** as metric. For all faces $f_j{'} \in \mathcal{L}_0{'}$ we compute the area deviation $\eta\left(f_j{'}\right)$ using Equation 7. We then aggregate the results into bins of size 0.2 and plot the resulting histogram. As shown in Figure 10, in all four datasets at least 43% of projected faces have areas that deviate less than 20%. This clearly indicates that our technique only introduces minor distortions.

8 LIMITATIONS

Our technique has some limitations that are discussed in the following. First of all, it slices the placenta in a discrete manner. A continuous layer definition is desirable in order to display the details between the layers. Such a continuous definition, however, was not in the focus of this work.

In general, our distance field-based solution extracts the offset surfaces while avoiding self-intersections. However, the topology of deeply located layers changes as the placenta thickness varies. By correcting the distance field using the information derived from the medial axis surface, it could be possible to preserve the topology. However, this requires further exploration and investigation.
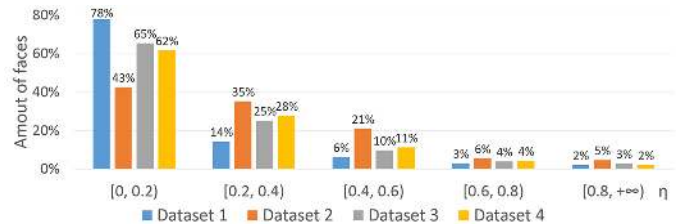
In our splitting step, the distance term of the cost function is increased incrementally with every face in the breadth-first traversal. Currently, the cost function does not consider the area of a face, which is considered a future aspect. As confirmed by the positive feedback of our collaborating clinical experts, our approach delivered satisfactory results for all presented datasets.

The ultimate goal of placenta maps is to aid researchers in the examination of placentas and to compare them in large population studies. With placenta maps, this now seems feasible. It is still an open topic how the comparison should be performed. Our technique cannot yet be utilized to create precise matches between multiple placentas, as there are currently no landmarks detected to align the compass overlay. Techniques from comparative visualization can be used to improve the compass overlay functionality with respect to multiple placentas. To validate and further improve our technique, larger user studies have yet to be carried out.

9 CONCLUSION AND FUTURE WORK

In this work, we presented placenta maps, a novel technique to visualize the in utero placenta in MRI data. It features an automatic reformation of the placenta into the fetal and maternal side, which creates occlusion-free 2D views respectively. In addition, it enables structure-aware slicing, which shows the internal tissues, and also the anatomical context of the placenta. The positive outcome of our conducted survey indicates that our technique may open new possibilities for in utero placenta examinations.

We see several directions for future work. One of the most interesting extensions is to integrate secondary tissue information, for example obtained by diffusion weighted imaging. According to the experts, the ability to compare the entire surface of multiple placentas is highly relevant and potentially will increase our understanding of the placental attachment to the uterine wall.

REFERENCES

[1] C. Menendez, J. Ordi, M. R. Ismail, P. J. Ventura, J. J. Aponte, E. Kahigwa, F. Font, and P. L. Alonso, "The impact of placental malaria on gestational age and birth weight," *Journal of Infectious Diseases*, vol. 181, no. 5, pp. 1740–1745, 2000.

[2] F. Arias, L. Rodriquez, S. C. Rayne, and F. T. Kraus, "Maternal placental vasculopathy and infection: Two distinct subgroups among patients with preterm labor and preterm ruptured membranes," *American Journal of Obstetrics and Gynecology*, vol. 168, no. 2, pp. 585–591, 1993.

[3] K. O'Donnell, T. O'Connor, and V. G. Glover, "Prenatal stress and neurodevelopment of the child: Focus on the HPA axis and role of the placenta," *Developmental Neuroscience*, vol. 31, pp. 285–292, 2009.

[4] D. J. Barker, A. R. Bull, C. Osmond, and S. J. Simmonds, "Fetal and placental size and risk of hypertension in adult life," *British Medical Journal*, vol. 301, no. 6746, pp. 259–262, 1990.

[5] K. Benirschke, G. J. Burton, and R. N. Baergen, *Pathology of the Human Placenta.* Springer Science & Business Media, 2012.

[6] M. Termeer, J. O. Bescós, M. Breeuwer, A. Vilanova, F. Gerritsen, and E. Gröller, "CoViCAD: Comprehensive visualization of coronary artery disease," *IEEE Transactions on Visualization and Computer Graphics*, vol. 13, no. 6, pp. 1632–1639, 2007.

[7] H. Miao, G. Mistelbauer, C. Nasel, and M. E. Gröller, "Visual quantification of the Circle of Willis: An automated identification and standardized representation," *Computer Graphics Forum*, 2016.

[8] L. Saroul, "Surface extraction and flattening for anatomical visualization," PhD thesis, Ecole Polytechnique Federale De Lausanne, 2006.

[9] B. Preim and C. P. Botha, *Visual Computing for Medicine.* Elsevier, 2013.

[10] J. Kretschmer, G. Soza, C. Tietjen, M. Suehling, B. Preim, and M. Stamminger, "ADR - Anatomy-Driven Reformation," *IEEE Transactions on Visualization and Computer Graphics*, vol. 20, no. 12, pp. 2496–2505, 2014.

[11] G. Mistelbauer, A. Morar, A. Varchola, R. Schernthaner, I. Baclija, A. Köchl, A. Kanitsar, S. Bruckner, and E. Gröller, "Vessel Visualization using curvicircular feature aggregation," *Computer Graphics Forum*, vol. 32, no. 3pt2, pp. 231–240, 2013.

[12] M. S. Floater, "Parametrization and smooth approximation of surface triangulations," *Computer Aided Geometric Design*, vol. 14, no. 3, pp. 231–250, 1997.

[13] A. Kanitsar, D. Fleischmann, R. Wegenkittl, P. Felkel, and M. E. Gröller, "CPR – Curved Planar Reformation," in *Proceedings of IEEE Visualization*, 2002, pp. 37–44.

[14] A. Vilanova, R. Wegenkittl, A. König, and M. E. Gröller, "Nonlinear virtual colon unfolding," in *Proceedings of IEEE Visualization*, 2001, pp. 411–418.

[15] M. Krone, F. Frieß, K. Scharnowski, G. Reina, S. Fademrecht, T. Kulschewski, J. Pleiss, and T. Ertl, "Molecular surface maps," *IEEE Transactions on Visualization and Computer Graphics*, vol. 23, no. 1, 2016.

[16] B. Ertl-Wagner, A. Lienemann, A. Strauss, and M. F. Reiser, "Fetal magnetic resonance imaging: indications, technique, anatomical considerations and a review of fetal abnormalities," *European Radiology*, vol. 12, no. 8, pp. 1931–1940, 2002.

[17] M. C. Frates, A. J. Kumar, C. B. Benson, V. L. Ward, and C. M. Tempany, "Fetal anomalies: Comparison of MR imaging and US for diagnosis," *Radiology*, vol. 232, no. 2, pp. 398–404, 2004.

[18] L. Manganaro, F. Fierro, A. Tomei, L. La Barbera, S. Savelli, P. Sollazzo, M. Eleonora Sergi, V. Vinci, L. Ballesio, and M. Marini, "MRI and DWI: feasibility of DWI and ADC maps in the evaluation of placental changes during gestation," *Prenatal Diagnosis*, vol. 30, no. 12-13, pp. 1178–1184, 2010.

[19] N. Linduska, S. Dekan, A. Messerschmidt, G. Kasprian, P. Brugger, K. Chalubinski, M. Weber, and D. Prayer, "Placental pathologies in fetal MRI with pathohistological correlation," *Placenta*, vol. 30, no. 6, pp. 555–559, 2009.

[20] M. Bouyssi-Kobar, A. J. du Plessis, R. L. Robertson, and C. Limperopoulos, "Fetal magnetic resonance imaging: exposure times and functional outcomes at preschool age," *Pediatric Radiology*, vol. 45, no. 12, pp. 1823–1830, 2015.

[21] M. M. Cannie, F. De Keyzer, S. Van Laere, A. Leus, J. de Mey, C. Fourneau, F. De Ridder, T. Van Cauteren, I. Willekens, and J. C. Jani, "Potential heating effect in the gravid uterus by using 3-T MR imaging protocols: Experimental study in miniature pigs," *Radiology*, vol. 279, no. 3, pp. 754–761, Dec 2016.

[22] C. Malamateniou, S. J. Malik, S. J. Counsell, J. M. Allsop, A. K. McGuinness, T. Hayat, K. Broadhouse, R. G. Nunes, A. M. Ederies, J. V. Hajnal, and M. A. Rutherford, "Motion-compensation techniques in neonatal and fetal MR imaging," *American Journal of Neuroradiology*, vol. 34, no. 6, pp. 1124–1136, 2012.

[23] B. Kainz, A. Alansary, C. Malamateniou, K. Keraudren, M. Rutherford, J. V. Hajnal, and D. Rueckert, *Flexible Reconstruction and Correction of Unpredictable Motion from Stacks of 2D Images.* Springer International Publishing, 2015, pp. 555–562.

[24] B. Kainz, M. Steinberger, W. Wein, M. Murgasova, C. Malamateniou, K. Keraudren, T. Torsney-Weir, K., P. Aljabar, M. Rutherford, J. Hajnal, and D. Rueckert, "Fast volume reconstruction from motion corrupted stacks of 2D slices," *IEEE Transactions on Medical Imaging*, vol. 34, no. 9, pp. 1901–1913, 2015.

[25] G. N. Stevenson, S. L. Collins, J. Ding, L. Impey, and J. A. Noble, "3-D ultrasound segmentation of the placenta using the random walker algorithm: Reliability and agreement," *Ultrasound in Medicine & Biology*, vol. 41, no. 12, pp. 3182–3193, 2015.

[26] G. Wang, M. A. Zuluaga, R. Pratt, M. Aertsen, A. L. David, J. Deprest, T. Vercauteren, and S. Ourselin, "Slic-Seg: slice-by-slice segmentation propagation of the placenta in fetal MRI using one-plane scribbles and online learning," in *Proceedings of Medical Image Computing and Computer-Assisted Intervention*, 2015, pp. 29–37.

[27] A. Alansary, K. Kamnitsas, M. Rajchl, A. Davidson, R. Khlebnikov, C. Malamateniou, M. Rutherford, J. Hajnal, B. Glocker, D. Rueckert, and B. Kainz, "Fast fully automatic segmentation of the human placenta from motion corrupted MRI," in *International Conference on Medical Image Computing and Computer-Assisted Intervention*. Springer, 2016, pp. 589–597.

[28] A. Alansary, B. Kainz, M. Rajchl, M. Murgasova, M. Damodaram, D. F. Lloyd, A. Davidson, S. G. McDonagh, M. Rutherford, J. V. Hajnal, and D. Rueckert, "PVR: Patch-to-Volume Reconstruction for large area motion correction of fetal MRI," 2016, preprint available on arXiv:1611.07289.

[29] R. Redline, D. Heller, S. Keating, and J. Kingdom, "Placental diagnostic criteria and clinical correlation - a workshop report," *Placenta*, vol. 26, Supplement, pp. S114 – S117, 2005.

[30] H. S. Wong, Y. K. Cheung, J. Zuccollo, J. Tait, and K. C. Pringle, "Evaluation of sonographic diagnostic criteria for placenta accreta," *Journal of Clinical Ultrasound*, vol. 36, no. 9, pp. 551–559, 2008.

[31] P.-E. Danielsson, "Euclidean distance mapping," *Computer Graphics and Image Processing*, vol. 14, no. 3, pp. 227–248, 1980.

[32] T.-C. Lee, R. L. Kashyap, and C.-N. Chu, "Building skeleton models via 3-D medial surface/axis thinning algorithms," *Graphical Models and Image Processing*, vol. 56, no. 6, pp. 462–478, 1994.

[33] M. S. Floater, "Mean value coordinates," *Computer Aided Geometric Design*, vol. 20, no. 1, pp. 19–27, 2003.

[34] The CGAL Project, *CGAL User and Reference Manual*, 4.9 ed. CGAL Editorial Board, 2016. [Online]. Available: http://doc.cgal.org/4.9/Manual/packages.html

Haichao Miao is a Ph.D. student at the Institute of Computer Graphics and Algorithms, TU Wien and at the Austrian Institute of Technology, Austria. His research interests include visualization of bio nanostructures and medical visualization.

Gabriel Mistelbauer is a postdoctoral researcher at the Otto-von-Guericke University Magdeburg, Germany since 2016. Before, he was a postdoctoral researcher at TU Wien, Austria, where he received a Ph.D. (2013) in computer science and a Master's degree (2010) in visual computing. His research mainly focuses on medical visualization, especially visual analysis of blood vessels and therapy planning.

Alexey Karimov was a project assistant at the TU Wien. He holds a MSc and Ph.D. in computer science. His research interests include topology, probability theory, real-time rendering, scientific and medical visualization.

Amir Alansary is a Ph.D. student in the Department of Computing at Imperial College London, UK. His research interests focus on Machine Learning, Medical Imaging and Computer Vision with specific emphasis on 3D medical image analysis including segmentation, motion compensation and super-resolution.

Alice Davidson is a part time data analyst, involved in many projects at the centre for the developing brain at Kings College London. She focuses her time on fetal volumetric reconstructions and segmentation, as well as conducting eye-tracking assessments for ex fetal participants as part of a follow up study. She is also in a training to be a mental health practitioner at Sussex University.

David F. A. Lloyd is a registrar in Paediatric Cardiology based at the Evelina Childrens Hospital, London. He is currently studying for a Ph.D. in advanced fetal imaging at the Division of Imaging Sciences and Biomedical Engineering, Kings College London.

Mellisa Damodaram is an Obstetrics and Gynaecology trainee with an interest in Maternal and Fetal Medicine. Her Ph.D. was on the use of Fetal MRI in foetuses with growth restriction at Imperial College London.

Lisa Story is currently a King's Open Prize Postdoctoral Research Fellow in the Centre for the Developing Brain St Thomas' Hospital (King's College London) having previously completed her Ph.D. at Imperial College London in the field of Magnetic Resonance Spectroscopy in growth restricted fetuses. She is also a senior obstetric registrar in the London deanery.

Jana Hutter did her undergraduate degrees in applied mathematics and received a Ph.D. from the University of Erlangen-Nuremberg in 2014. Since 2014 she is an associate researcher at the Centre for the Developing Brain at King's College London. Her interests include MRI physics, sequence development, diffusion MRI as well as fetal/placental and neonatal imaging.

Joseph V. Hajnal is Professor of Imaging Sciences at Kings College London. He trained as a physicist at Bristol University, England, UK and obtained a Ph.D. in the physics of electromagnetic waves before working in Australia at Melbourne University and the ANU on interactions between atomic beams and laser light. In 1990 he began research in medical imaging. His research group focuses on in vivo imaging, particularly Magnetic Resonance Imaging (MRI). His current research interests include MR data acquisition and processing, image registration and data fusion as well as novel scanner technology, parallel imaging and motion artefact correction. He has invented and pioneered techniques that are now widely used in the medical imaging industry. With Daniel Rueckert, he co-founded a IXICO and also developed the critical motion-tolerant imaging methods that underpin image acquisition in this programme.

Mary Rutherford is Professor of Perinatal Imaging at Kings College London, and is based within the Centre for the Developing Brain at St Thomas Hospital. She is also an Honorary Professor at Stellenbosch University. She originally trained as a paediatrician, specialised in neonatal neurology and became involved in MRI in the late 1980s. She has since worked as a clinical researcher in the field of MRI. Initially studying acquired injury in the term and preterm neonatal brain and since 2002 assessing congenital and acquired abnormalities using fetal MRI. More recently she has started working on imaging the placenta, being PI on an NIH funded project to study placental structure and function with MRI.

Bernhard Preim heads the Visualization Group at the University of Magdeburg (UoM), Germany since 2003. Before, he was a staff member at MEVIS Bremen, Germany. He received a Ph.D. at the UoM in 1998 and a habilitation (venia legendi) in 2002 from the University of Bremen.

Bernhard Kainz is Lecturer in the Department of Computing at Imperial College London. He is researching translational high-performance medical data analysis, machine learning, and interactive real-time image processing techniques as member of the Biomedical Image Analysis, BioMedIA Group in the section of Visual Information Processing. He is honorary research fellow at Kings College London, Division of Imaging Sciences and Biomedical Engineering, St. Thomas Hospital London and collaborates intensively with the department of Bioengineering at Imperial.

M. Eduard Gröller is professor at TU Wien, Austria, and adjunct professor of computer science at the University of Bergen, Norway. His research interests include computer graphics, visualization and visual computing. Dr. Gröller became a fellow of the Eurographics association in 2009. He is the recipient of the Eurographics 2015 Outstanding Technical Contributions Award.